A Dam Spillway Model Using End Sill

Yogi Pandhu Satriyawan
Doctoral Program in Department of Water Resources, Faculty of Engineering, University of Brawijaya, Indonesia
pandhuyogi@gmail.com

Very Dermawan
Department of Water Resources, Faculty of Engineering, University of Brawijaya, Indonesia
peryderma@ub.ac.id

Pitojo Tri Juwono
Department of Water Resources, Faculty of Engineering, University of Brawijaya, Indonesia
pitojo_tj@ub.ac.id

Dian Sisinggih
Department of Water Resources, Faculty of Engineering, University of Brawijaya, Indonesia
singgih@ub.ac.id

Lily Montarcih Limantara
Department of Water Resources, Faculty of Engineering, University of Brawijaya, Indonesia
lilymont@ub.ac.id (corresponding author)

Received: 15 June 2025 | Revised: 15 July 2025 and 3 August 2025 | Accepted: 11 August 2025

 DOI: https://doi.org/10.48084/etasr.12753

ABSTRACT

This research focuses on the development of a hydraulic model of energy dissipator with segmented end sill on the dam spillway as a modification of the standard United States Bureau of Reclamation (USBR) Type III design. By using Froude similarity analysis at 1:100 scale and a Froude number range of 13-25, this study compares the performance of the standard design (Configuration A) with a modification by using a two-segment zigzag pattern segmented end sill (Configuration B). The results show that Configuration B achieves a specific energy reduction of up to 15- 23% higher than Configuration A across all tested discharge ranges (9-22 l/s). The segmented end sill causes the increase of turbulence, the expansion of the vortex area, a more even distribution of energy, and then the reduction of the potential damage in the dam downstream. This research provides an efficient and economical design alternative for improving the safety of hydraulic structures in dams with high supercritical flow conditions.

Keywords-energy dissipator; segmented end sill; dam spillway; Froude number; USBR type III

I. INTRODUCTION

Dam is a water resource infrastructure, which is important and beneficial to the society. In addition, it is useful for increasing the socio-economic status by the self-reliance on the food production, irrigation, conservation efforts, hydro-electric power production, flood control, tourism, and others [1]. Although dams help the societal development, they are also vulnerable to damage, causing a fast and uncontrolled water release [2, 3]. The dam break is considered a big disaster with a significantly negative impact on the economics, society, and environment; so it must be prevented [4]. The stilling basin is a significant component in the dam infrastructure, which dissipates the more kinetic energy from the supercritical flow that traverses the spillway before being released to the downstream channel. Flow with high kinetic energy has potential to cause scouring, river bed erosion, and structural damage if there is no effective dissipation this this energy [5]. Stilling basin design standards, such as USBR Type III, developed by the USBR has been widely used for the flow conditions with the high Froude number ($Fr > 4.5$),. However, research shows that the structural modification can significantly improve the energy dissipation efficiency [6, 7]. For high energy flow, conventional energy dissipaters, such as USBR Type III stilling basin, often become less effective or need a very big size of stilling basin. To overcome these challenges, an energy dissipator with an innovative design is needed to increase the efficiency and control the hydraulic jump, ensuring stability and compactness in the stilling basin.

This research aims provide a solution to these challenges by modifying the energy dissipator through additional sequent end sill. The study involves placing one or more additional crests strategically in the standard stilling basin to force the more effective form of hydraulic jump, to intensify the formation of macro turbulence, and create more efficient multi-stage energy dissipators compared to the conventional single jump. It has been shown that the increase of turbulence and the interruption of the flow structure can significantly increase the energy dissipation [8, 9]. Authors in [10] demonstrated that the geometric modifications can increase the dissipation efficiency by up to 30% for the high Froude number flow. Meanwhile, authors in [11] reported that the use of segmented end sill can increase the length of the hydraulic jump by 25% compared to the conventional design. However, research related to the use of segmented end sill with a zigzag pattern on the high supercritical flow ($Fr > 10$) is still relatively limited, especially in the context of its application in the large-scaled dam.

This research uses a physical model with the scale of 1: 100, based on the similarity analysis of Froude, with the Froude number ranging from 13 to 25, to compare the performance of a Type III standard USBR energy dissipator (Configuration-A) and a modified one using a segmented end sill in a two-segment zigzag pattern (Configuration B). The analyzed parameters include the specific energy, hydraulic jump characteristic, velocity profile, and pressure distribution on the channel bed. The findings of this study aid in more efficiently designing dam energy dissipators with high supercritical flow. Also, comprehensive empirical data for the validation of the numerical model are provided along with the development of a hydro-dynamic theory for hydraulic jump under extreme conditions.

II. MATERIALS AND METHODS

A. Spillway

Every reservoir has a certain storage capacity for holding water. When the storage is full, the reservoir level rises and the water overflows through the dam crest. To prevent this overflow, spillways are required to safely release the water into the downstream. The spillway can be constructed separately or integrated into the dam body. The optimal design of the spillway channel is very important as a suboptimal design may cause erosion on the downstream side [12]. The spillway structure can either be controlled or uncontrolled, depending on the field condition. The controlled spillway channel is built with a gate that can be raised or lowered according to the reservoir operations during flooding. In contrast, the uncontrolled spillways have no gates; the water simply flows over the crest and into the spillway, depending on the water level.

B. Basic Principle of Energy Dissipators on the Dam Spillway

The energy dissipator on the dam spillway works by transforming the supercritical flow with high velocity to the sub-critical flow through the hydraulic jump. The conventional energy dissipator consists of the stilling basin, chute blocks, baffle blocks, and end sill that synergistically works to maximize the energy dissipation [13, 14].

The mechanism of the energy dissipation through the hydraulic jump is [10]:

- The formation of turbulence with high intensity
- The friction of the internal fluid
- Air entrainment
- The interaction between the flow and barrier structure

The effectiveness of the energy dissipator is generally evaluated based on the ratio of the energy dissipation achieved, the stability of the hydraulic jump, and the length of the hydraulic jump with respect to the dimensions of the stilling basin.

C. Classification of USBR-Energy Dissipator

USBR has classified types of standard energy dissipators that are widely used. The USBR-energy dissipator Type III discussed this research is specially designed for the flow conditions with a Froude number over 4.5 and a very high flow velocity [15]. Authors in [16] demonstrated that the geometric modification of end sill can generate three dimension-flows, which increase the mixing and energy dissipation. A combination of PIV and Large Eddy Simulation (LES) was used to analyze the structure of turbulence forming on the re-circulation zone. Authors in [5] studied the evolution of the energy dissipator design and concluded that although the standard design of USBR had been optimized, there is a significant potential for further improvement, particularly regarding the field condition with high Froude number ($Fr >$ 10), as often seen in the high dam. Authors in [17] reported that the use of end sill with fractal geometry can increase the efficiency of the energy dissipator by 35% compared with the conventional design on the high Froude number ($Fr > 15$). This study uses turbulence spectral analysis for identifying the mechanism of energy transfer from larger to smaller scales.

D. Modification of End Sill and its Influence on Energy Dissipation

Authors in [9] demonstrated that the use of a jagged end sill can increase the energy dissipation by 15% compared to the conventional end sill for the flow with a Froude number between 4 and 8 by expansion of the lateral flow and the increase in turbulence. Authors in [8] showed that a non-conventional geometry can significantly influence the characteristics of turbulent flow and the re-circulation pattern in a stilling basin, resulting in improved energy dissipation efficiency and better protection of the downstream channel bed. Authors in [18] developed the model of an end sill with a stepped configuration, which improved the energy dissipation by about 20% compared to the conventional design for a flow with a high Froude number. The study also demonstrated that the optimization of the slope angle and the relative height of the end sill can significantly influence the overall performance of the energy dissipator.

E. Physical Modeling of Hydraulic Structure

Physical modeling has remained the main method for validating and developing the hydraulic structure design, although significant progress has been achieved in numerical

modeling [19]. To accurately replicate the hydro-dynamic behavior, authors in [20] applied Froude similarity analysis to ensure the ratio of inertial force to the gravitational force in the model matches that of the actual prototype [21]. Authors in [21] underlined the importance of hybrid approaches that combine the physical and numerical modeling for optimizing the design of complex hydraulic structures. However, for complex turbulence flow such as a hydraulic jump under high Froude number, the physical modeling has remained the most reliable approach for flow characterization and validation of design concept [22].

F. Methodology

1) Design of the Physical Model

This study was conducted on a physical model at a scale of 1: 100, based on the Froude similarity analysis [20]. The model, as shown in Figure 1, was designed to simulate the flow on the dam spillway with a Froude number from 13 to 25. The hydraulic model test of the energy dissipator using sequent end sill was conducted in the Laboratory of River Engineering, Department of Water Resources, Faculty of Engineering, University of Brawijaya, Malang, Indonesia. The model installations consist of :

- System of water supply: The reservoir has a capacity of 5,000 L with a 25-kW centrifugal pump, and an automatic discharge control system with an electro-magnetic valve of ±0.5% accuracy.
- Ogee-spillway: The ogee spillway is a hydraulic structure designed to discharge the surplus water from the dam with an S-curve profile that follows the free-fall water-flow form (nape) [23, 24]. It was designed with 100 cm depth to maximize the discharge efficiency by minimizing the cavitation and negative pressure on the structure.
- Stilling basin: The stilling basin is 1000 cm × 40 cm × 50 cm in size with a transparent acrylic bed for observation.

Fig. 1. Physical model setup of the dam spillway with energy dissipator.

2) Froude Number

Froude number is a non-dimensional parameter representing the relation between the inertial and gravitation force in the water flow. The wave length is equal to the hydraulic depth [24]. The Froude number can be calculated using:

$$Fr = \frac{v}{\sqrt{(g \times d)}} \quad (1)$$

where V is the flow velocity in m/s, g is the acceleration due to gravity in m/s^2, and d is the flow depth in m.

- If $Fr < 1$: The gravitational force is dominant and the flow is sub-critical.
- If $Fr > 1$: The inertial force is more dominant and the flow is super-critical.

The Froude number is used to determe the flow type [25]. For the sub-critical flow, the boundary condition is located downstream, while for the super-critical condition, the boundary condition is located upstream. When $Fr = 1$, the flow is critical [24]. To match the flow conditions in the model with those in the prototype, the Froude number in the prototype (Fr_p) must be the same as the Froude number in the model (Fr_m). The ratio (scale) of the Froude number in the prototype to that in the model can be expressed as:

$$n_{Fr} = \frac{Fr_p}{Fr_m} = \frac{\left[\frac{v}{\sqrt{g \times h}}\right]_p}{\left[\frac{v}{\sqrt{g \times h}}\right]_m} \quad (2)$$

Based on (2), the scale of flow velocity can be presented as:

$$\left[\frac{v}{\sqrt{g \times h}}\right]_p = \left[\frac{v}{\sqrt{g \times h}}\right]_m;$$

$$\left[\frac{v}{\sqrt{g_p \times h_p}}\right]_p = \left[\frac{v}{\sqrt{g_m \times h_m}}\right]_m \frac{v_p}{v_m} = \left(\frac{g_p}{g_m}\right)^{\frac{1}{2}} \times \left(\frac{h_p}{h_m}\right)^{\frac{1}{2}}$$

As $g_p = g_m$, then $n_g = 1$. Therefore:

$$n_v = (n_h)^{\frac{1}{2}}$$

3) Time of Flow

The time required for a water particle to travel under uniform motion is expressed as:

$$Time\ (t) = \frac{distance\ (L)}{velocity\ (v)}$$

For the scale model without distortion, the time is obtained as:

$n_t = \frac{n_L}{n_v}$ and $n = (n_h)^{\frac{1}{2}}$, so:

$$n_t = (n_h)^{\frac{1}{2}}$$

4) Flow Discharge

The discharge can be calculated using the continuity equation:

$$Q = V \times A$$

where A is the wet cross section area ($A = L \times h$). The relation can then be expressed as:

$$n_Q = n_v \times n_A$$

$$n_v = (n_h)^{1/2}$$

$$n_A = n_L \times n_h$$

For the scale model without distortion, $n_L = n_h$, so:

$$n_A = (n_h)^2$$

Thus:

$$n_Q = (n_h)^{5/2}.$$

5) Segmented End Sill

The design of the segmented end sill was selected to match with a barrier block of USBR Type III. In this study, the segmented end sill is placed at the center of the energy dissipator as the water flow regulator. After passing the segmented end sill, the flow becomes sub-critical.

6) Configuration of Test and Parameter

Two configurations of energy dissipators were tested in this research:

- Configuration-A: Standard Type III USBR energy dissipator, with dimensions in accordance with the USBR design guidelines [10]: 1) height of chute blocks =0.724 m, 2) height of baffle blocks = 2.515 m, and 3) height of end sill = 1.5 m.
- Configuration-B: Modified Type III USBR energy dissipator with segmented end sill and zigzag pattern consisting of two segments: 1) distance between end sill segments = 5 m from baffle blocks, 2) height of baffle blocks (n_3) = 2.515 m, and 3) distance between segment = $0.75 \times n_3 = 1.886$ m.

7) Testing Parameter

Testing was carried out for the following discharge variations: 9 L/s, 11 L/s, 13 L/s, 15 L/s, 17 L/s, 19 L/s, 20 L/s, and 21 L/s. For every combination of the configuration and discharge, the following parameters were measured and analyzed:

- Profile of water level along the stilling basin
- Initial and final depth of hydraulic jump
- Length of hydraulic jump
- Velocity profile on the key locations
- Pressure distribution on the stilling basin bed
- Specific energy upstream and downstream of the energy dissipator

8) Equipment and Measurement Technique

The water depth was measured using an automatic water-level device, providing ±0.1 cm accuracy, at three points along the longitudinal axis of the stilling basin. The velocity profile was measured using Pitot Tube on the three key locations (0.2b, 0.5b, and 0.8b, where b is the channel width). The pressure distribution on the spillway channel bed was measured using piezometers with ±0.01 kPa accuracy, relative to the channel bed surface. The flow visualization is carried out using a smartphone camera recording at 60 fps.

9) Determination of Model Scale

The model scale for testing is determined using the factors: a) the aim of testing, b) the desired accuracy, c) the facilities available in the laboratory, and d) the time and cost. Based on these parameters, a geometric scale of 1:50 was used in this study, and the related model dimensions are presented in Table I.

TABLE I. MODEL DATA

Parameter	Notation	Formula	Example (for n_h=n_L=50)
Flow velocity	v	$n_v = (n_h)^{1/2}$	n_v=7.071
Flow time	t	$n_t = n_h^{1/2}$	n_t=7.071
Discharge	Q	$n_Q = (n_h)^{5/2}$	n_Q=17677.670
Diameter	d	$n_d = n_h$	n_d=50
Volume	V	$n_V = n_h^3$	n_V=125.000
Chezy coefficient	C	$n_C = 1$	n_C=1
Manning's Coefficient	n	$n_n = n_h^{1/6}$	n_n=1.9194

10) Data Analysis

The data were analyzed to determine the following parameters:

1. Efficiency of energy dissipator (η):

$$\eta = \frac{(E_1 - E_2)}{E_1} \times 100\%$$

where E_1 and E_2 are the energies upstream and downstream of the energy dissipator, respectively, and can be calculated using:

$$E = y + \frac{V^2}{2g}$$

where y is the depth of water, V is the average velocity, and g is the acceleration due to gravity.

2. Relative length of hydraulic jump (R_L):

$$R_L = \frac{L_j}{y_2}$$

where L_j is the length of hydraulic jump and y_2 is the conjugate depth on the downstream.

3. Intensity of turbulence, is analyzed from the fluctuation of velocity measured using ADV.

4. Coefficient of pressure in the bed (C_p):

$$C_p = \frac{(p - p_0)}{(0.5\rho V^2)}$$

where p is the measurable pressure, p_o is the reference pressure, ρ is the density of water, and V is the reference velocity.

III. RESULTS AND DISCUSSION

A. Flow Characteristic on the Energy Dissipator

The visual observations revealed a significant difference in the flow structure between the two configurations. In Configuration-A (standard Type III USBR), the hydraulic jump is formed with the conventional characteristics that include a clear roller surface and a single circulation zone. On the contrary, Configuration-B (with segmented end sill) exhibited fragmentation of the lateral flow that formed multiple vortices and increased the complexity of the three-dimensional flow.

The sample calculation for the depth and Froude number at a discharge of 13 *L/s* is:

Data used: Q = 13 *L/s* = 0.013 m/s, B = 0.40 m, Y_1 = 0.0072 m

- Unit discharge:

$$q = \frac{Q}{B} = 0.0013/0.40 = 0.0325 \text{ m}^2/\text{s}$$

- Critical depth:

$$Yc = (\frac{q^2}{g})^{1/3} = (\frac{0.013^2}{9.81})^{1/3} = 0.048 \text{ m}$$

- Specific energy at the critical depth:

$$E_0 = E_C = 1 + \frac{3}{2} Y_C = 1 + \frac{3}{2\ 0.048} \times 0.048 = 1.06 \text{ m}$$

- Critical velocity:

$$V_C = \frac{q}{Y_C} = \frac{0.0325}{0.048} = 0.68 \text{ m/s}$$

- Velocity at depth Y_1:

$$V_{y_1} = \frac{q}{Y_C} = \frac{0.0325}{0.072} = 4.49 \text{ m/s}$$

- Froude number at Y_1:

$$F_{y_i} = \frac{V}{\sqrt{g.H}} = \frac{4.49}{\sqrt{9.81.0.0072}} = 16.84$$

- Specific energy at Y_1:

$$E_1 = Y_1 + \frac{v^2}{2.g} = 0.0072 + \frac{0.68^2}{2.9.81} = 1.03 \text{ m}$$

- Conjugate depth Y_2:

$$Y_2 = \frac{Y_1}{2x\sqrt{(1+8{F_1}^2)}} - 1 = \frac{0.0072}{2x}$$

$$Y_2 = \sqrt{(1 + 8.16.84^2)} - 1 = 0.1689 \text{ m}$$

- Velocity at depth Y_2:

$$V_{y_2} = \frac{q}{Y_C} = \frac{0.0325}{0.1689} = 0.19 \text{ m/s}$$

- Specific energy at Y_2:

$$E_2 = Y_2 + \frac{v^2}{2.g} = 0.1689 + \frac{0.19^2}{2.9.81} = 0.17 \text{ m}$$

- Efficiency of the dissipator (%):

$$\eta = \frac{(E_1 - E_2)}{E_2} \times 100\% = \frac{(1.03 - 0.17)}{0.17} \times 100\% = 83.49\%$$

- Efficiency of the dissipator using the critical energy (%):

$$\frac{(E_0 - E_2)}{E_2} \times 100\% = \frac{(1.07 - 0.17)}{0.17} \times 100\% = 84.06\%$$

In this physical model test, the spillway is of Ogee Type I.

B. Efficiency of Energy Dissipator

The design of the energy dissipator used in this study follows the standard criteria of USBR Type III, which is generally proposed for the flow with a Froude number (Fr_1) greater than 4.5. The geometric configuration of this energy dissipator includes the front block, hinder block, and end crest, which were determined based on the hydraulic parameters generated by the design discharge (Q_d = 13 L/s). Figure 2 illustrates the configuration of the standard USBR Type III energy dissipator.

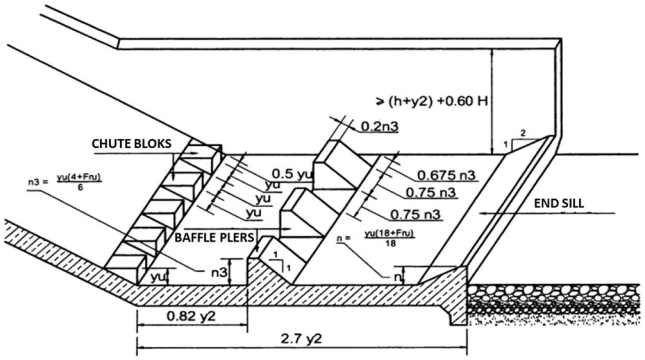

Fig. 2. Standard USBR Type III energy dissipator.

The schematics and dimensions of the USBR Type III energy dissipator were used as a reference for this study. The scaled-down geometric dimensions for every component of the physical model based on the hydraulic parameters from the design discharge are presented in Table II.

TABLE II. HYDRAULIC PARAMETER

Component	Formula	Prototype dimension (m)	Model dimension (cm)
Width of front block	y_u	0.724	0.724
Distance of front block and wall	0.5 y_u	0.362	0.362
Height of hinder block	n_3	2.515	2.515
Width of hinder block peak	0.2 n_3	0.503	0.503
Distance of hinder block and wall	0.675 n_3	1.698	1.698
Width of hinder block	0.75 n_3	1.886	1.886
Distance of hinder block and front block	0.82 y_2	13.847	13.847
Length of energy dissipator	2.7 y_2	45.594	45.594
Height of end crest	n	1.402	1.402

To obtain the dimensions of the physical model, each geometric dimension of the prototype was converted using the determined scale ratio. This study uses the scale of 1:100, which means that every dimension (length, width, height) of the model was 100 times smaller than that of the prototype. Configuration B demonstrates a significantly higher energy dissipation efficiency compared with Configuration A, highlighting its superior performance. Figure 3 presents a sectional view of the USBR Type II stilling basin (Configuration B), Figure 4 shows a longitudinal view of the basin with the dam, and Figure 5 illustrates a side view of the USBR Type II stilling basin.

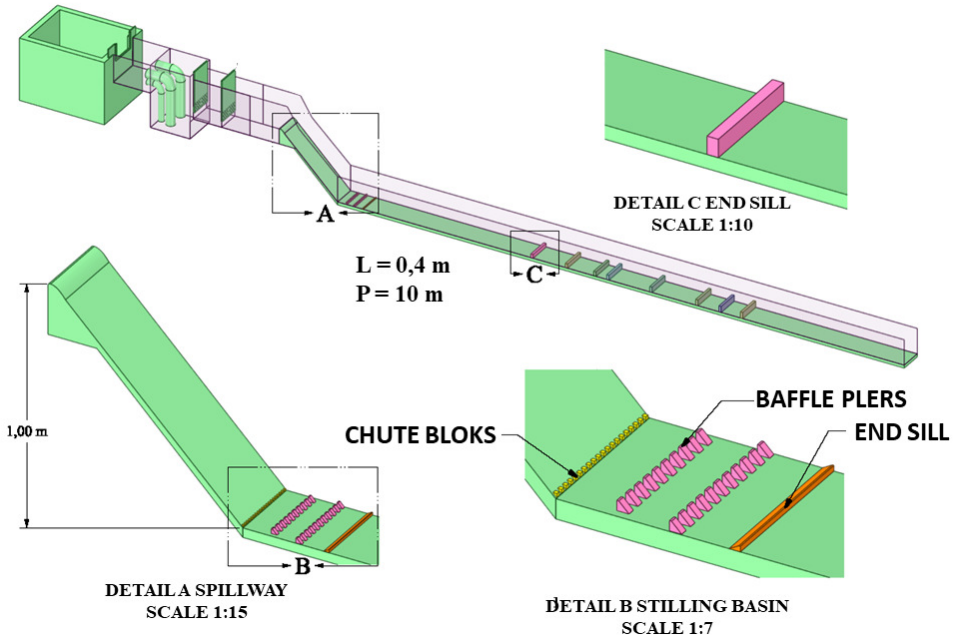

Fig. 3. Sectional view of USBR Type II stilling basin (Configuration B).

Fig. 4. Longitudinal view of USBR Type II stilling basin with dam (Configuration B).

Fig. 5. Side View of USBR Type II stilling basin (Configuration B).

Before analyzing the water level profile, it is required to identify and measure the length of the hydraulic jump. This measurement is crucial for understanding the scale and position of the main energy dissipator. For each test discharge on the USBR Type III energy dissipator, measurements were carried out for three main distance parameters: X_1, X_2, and L_j. Figure 6 provides a schematic representation of the distance measuring parameter.

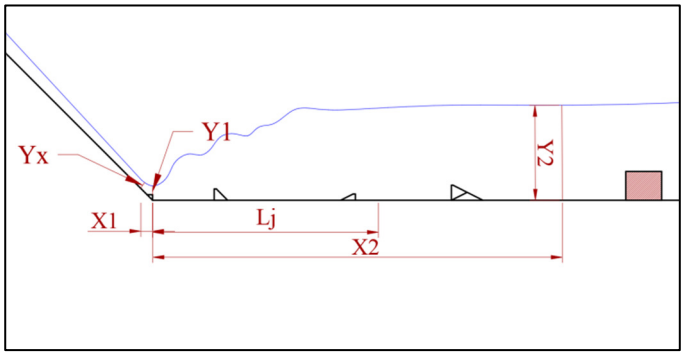

Fig. 6. Schematic illustration of initial jump distance (X_1), end jump distance (X_2), and length of the hydraulic jump (L_j).

The initial jump distance (X_1) is the horizontal distance measured from the spillway foot (start of the stilling basin) to the point where the stilling water from the energy dissipator begins to meet the supercritical flow from the chute way. This point, located at the toe, marks the start of the hydraulic jump and is where the initial flow depth (Y_x) is measured on the slanted cross section.

The end jump distance (X_2) is the horizontal distance measured from the spillway foot to the point where the hydraulic jump is fully developed. This point is also visually located at a relatively stable water surface where the turbulence and air bubbles start decreasing. This point marks the location of the depth of the sub-critical flow (Y_2).

The length of the hydraulic jump (L_j) is the effective length of the jump, calculated as the difference between the end jump distance (X_2) and the initial jump distance (X_1).

C. Velocity Profile and Turbulence Intensity

There is a substantial difference in the measured velocity distribution between Configuration-A and Configuration-B.

A sample calculation for the velocity profile analysis is:

Data (Serial-0): Q = 13 *L/s* at section Y_1, C_v = 0.9023, Δh = 30.1 cm, g = 9.81 m/s^2.

- Pitot tube velocity:

  $V_{pitot} = C_v \times \sqrt{2g \times \Delta h}$;

  $C_v \times \sqrt{2.981 \times 30.1} = 219.27$ cm/s.

- Average velocity:

  $V_{average} = \frac{V_{pitot\ left} + V_{pitot\ as} + V_{pitot\ right}}{3}$

  $\frac{219.27+224.31+229.27}{3} = 220.95$ cm/s

- Prototype velocity:

  $V_{prototype} = V_{average} \times \sqrt{scale} = 220.95 \times \sqrt{100}$;

  $2209.53\ cm/s = 22.10$ m/s.

- Flow type (Froude number) :

  $Fr = \frac{V}{\sqrt{g \times Hwater}} = \frac{22.48}{9.81 \times 2.37} = 4.35$ (Super critical).

Table III summarizes the analysis of the velocity, Froude number, and flow type. Configuration-B demonstrated sharper velocity gradient near the channel bed and the velocity is more evenly distributed on the upper profile. This indicates a turbulent flow and more effective momentum transfer compared to Configuration-A at the same location. This behavior confirms the hypothesis that the segmented end sill enhances the formation of turbulence and vortex structures. These findings are consistent with those in [22], where a strong correlation between the turbulence intensity and energy dissipation efficiency in hydraulic jumps was noted. The spectral analysis of the velocity fluctuation shows that Configuration-B produces a turbulent flow structure with wider frequency spectrum; it indicates a more effective energy transfer from large-scale to small-scale turbulent structures, where viscous dissipation occurs.

D. Pressure Distribution on the Stilling Basin Bed

1) Analysis of Pressure Coefficient

The pressure distribution coefficient (C_p) analysis on the stilling basin bed shows the significant difference between both configurations, especially on the region near the end sill.

In Configuration-A, the pressure distribution is relatively monotonous with a gradual increase towards the end sill. In contrast, Configuration-B exhibits a complex pressure distribution with greater spatial fluctuations, indicating a more complex three-dimensional flow structure.

The maximum C_p is consistently 15%–20% lower in Configuration-A than in Configuration-B, indicating the reduction in the intensity of the impact pressure on the bed. It is an important finding from the perspective of the structural design because the high impact pressure can cause damage on the concrete bed during the long-term operation.

2) Cavitation Risk Assessment

Using the cavitation index, $\sigma = \frac{(p - p_v)}{0.5\rho V^2} \times 2$, where p_v is the vapor pressure, the results presented in Table IV show that Configuration-B has a lower cavitation risk compared to Configuration-A. The minimum cavitation index for Configuration-B is 0.000298 and 0.000336 for Configuration-A, indicating that Configuration-B provides a greater safety margin against cavitation.

E. The Influence of Froude Number on the Relative Performance

The influence analysis based on the Froude number exhibited an interesting trend. The energy dissipation efficiency

of configuration-B consistently increases with the increase in the Froude number, from about 15% at $Fr \approx 13$ to more than 23% at $Fr \approx 25$. This result indicates that the modified segmented end sill is more effective under extreme super-critical flow conditions. This trend can be explained by the formation of secondary vortex structures, which become more intense at higher Froude numbers, as observed in the flow visualization. This is a significant finding as it helps mitigate the adverse effects of the high kinetic energy on the large dams.

TABLE III. SUMMARY OF VELOCITY, FROUDE NUMBER, AND FLOW TYPE FOR MODEL AND PROTOTYPE AT Q = 13 L/S

Section	Velocity (cm)			C_p	V for model (cm/s)			Average	V for prototype		H water	Fr	Type of flow
	Left	As	Right		Left	A_s	Right	(cm/s)	(cm/s)	(m/s)	m		
Y_C	1.5	1.4	1.5	0.98	53.16	51.36	53.16	52.56	525.64	5.26	3.39	0.91	Sub-critic
1	4.6	4.5	4.5	0.98	93.10	92.08	92.08	92.42	924.23	9.24	3.18	1.65	Super-critic
2	6.2	6.1	6.1	0.98	108.09	107.21	107.21	107.50	1075.03	10.75	2.75	2.07	Super-critic
3	8.0	8.1	8.0	0.98	122.78	123.54	122.78	123.03	1230.33	12.30	2.45	2.51	Super- critic
4	13.3	13.1	13.1	0.98	158.31	157.11	157.11	157.51	1575.11	15.75	2.00	3.55	Super-critic
5	20.5	20.4	21	0.98	196.54	196.06	198.92	197.17	1971.75	19.72	1.56	5.05	Super-critic
6	30.7	30.4	30.1	0.98	240.52	239.34	238.15	239.34	2393.36	23.93	1.27	6.77	Super-critic
7	39.5	44.5	43.5	0.98	272.82	289.57	286.30	282.90	2828.96	28.29	0.92	9.42	Super-critic
8	49.7	49.4	49.5	0.98	306.02	305.10	305.41	305.51	3055.09	30.55	0.85	10.59	Super-critic
9	51.3	51	50.9	0.98	310.91	310.00	309.70	310.20	3102.01	31.02	0.71	11.78	Super-critic
10	56	56.5	58.2	0.98	324.84	326.29	331.16	327.43	3274.29	32.74	0.55	14.08	Super-critic
Y_x	54.5	54.4	54.2	0.98	320.46	320.17	319.58	320.07	3200.68	32.01	0.63	12.88	Super-critic
Y_1	32	30	30.4	0.98	245.56	237.76	239.34	240.88	2408.84	24.09	2.50	4.86	Super-critic
Y_2	0.7	0.6	0.5	0.98	36.32	33.62	30.69	33.55	335.46	3.35	14.17	0.28	Sub-critic

TABLE IV. CAVITATION ON DISCHARGE OF 13 L/S

Section	ρw	h	P_g		P_a	P_0	P_v	V_0	$V_0^2/2$	ρ	C_p	Cavitation
	(kg/m^3)	(m)	(N/m2)	(kPa)	(kPa)	(kPa)	(kPa)	(m/dt)	(kg/m3)			
	1	2	3	4	5	6	7	8	9	10	11	12
Y_C	1019.8	3.390	33955.51	33.96	101	134.96	2.726	5.26	13.814624	0.009386	0.002410	Non-cavitation
1	1019.8	3.180	31833.29	31.83	101	132.83	2.726	9.24	42.709758	0.002987	0.000731	Non-cavitation
2	1019.8	2.750	27518.11	27.52	101	128.52	2.726	10.75	57.7844960	0.002135	0.000467	Non-cavitation
3	1019.8	2.450	24523.42	24.52	101	125.52	2.726	12.30	75.6855930	0.001591	0.000318	Non-cavitation
4	1019.8	2.000	20043.18	20.04	101	121.04	2.726	15.75	124.048480	0.000935	0.000158	Non-cavitation
5	1019.8	1.560	15562.94	15.56	101	116.56	2.726	19.72	194.389612	0.000574	0.000079	Non-cavitation
6	1019.8	1.270	12733.32	12.73	101	113.73	2.726	23.93	286.409681	0.000380	0.000044	Non-cavitation
7	1019.8	0.920	9196.284	9.200	101	110.20	2.726	28.29	400.151946	0.000263	0.000023	Non-cavitation
8	1019.8	0.850	8488.877	8.490	101	109.49	2.726	30.55	466.678749	0.000224	0.000018	Non-cavitation
9	1019.8	0.710	7074.065	7.070	101	108.07	2.726	31.02	481.124494	0.000215	0.000014	Non-cavitation
10	1019.8	0.550	5517.77	5.520	101	106.52	2.726	32.74	536.048178	0.000190	0.000010	Non-cavitation
Y_x	1019.8	0.630	6295.917	6.300	101	107.30	2.726	32.01	512.216181	0.000200	0.000012	Non-cavitation
Y_1	1019.8	2.500	25010.6	25.01	101	126.01	2.726	24.09	290.126298	0.000417	0.000085	Non-cavitation
Y_2	1019.8	14.17	141726.7	141.73	101	242.73	2.726	3.350	5.62654400	0.041827	0.024700	Non-cavitation

F. Practical Implications and Design Recommendations

Based on the analysis, the segmented end sill with a two-segment zigzag pattern (Configuration-B) provides a more promising design alternative for energy dissipation in dams subjected to highly super-critical flow conditions. The advantages of the modified stilling basin:

- Up to 23% higher energy dissipation efficiency under high Froude numbers.
- Up to 18% reduction in the hydraulic jump length, resulting in shorter stilling basin.
- More even distribution of pressure on the stilling basin bed, reducing the risk of structural damage.
- Higher hydraulic jump stability, especially during high discharge conditions.

Based on the comparative analysis of the two configurations, Configuration-B (USBR III with sequent end sill) was found to be the most effective and optimal design. This configuration is not only able to dissipate the energy effectively, but also ensures that the hydraulic jump remains completely within the safe stilling basin.

Configuration-B can be implemented with minimal additional costs on the new projects or as retrofitting on the existing structure, to improve the operational safety of the dam. The recommendations for practical implementation are:

- The optimal zig-zag angle should range between 30° to 45°.
- The ratio of segment height should be 0.7 to 1.0 of the conventional end sill height.
- The segment should be placed at an optimal distance of 0.3-0.5 times the channel width.

IV. CONCLUSION

This research investigates the hydraulic performance of an energy dissipator of segmented end sill with a zigzag pattern on

the dam spillway, in comparison with the performance of the standard United States Bureau of Reclamation (USBR) Type III design. The study employs a 1:100 scale physical model, tested across a Froude number range of 13-25. Based on the experimental results and comprehensive analysis, the following conclusions can be drawn:

- The modified segmented end sill with a segment zigzag pattern (configuration-B) exhibited increased energy dissipation efficiency of 15-23% over the conventional design (configuration-A), across the entire tested Froude number range.
- The hydraulic jump length in configuration B was 12–18% shorter than in configuration A, indicating a faster transition from the supercritical to the subcritical flow and allowing for a smaller stilling basin. It has been shown that Type II and III stilling basins reduce the length of the hydraulic jump by 50%-73%, respectively, while also lowering the flood potential [25].
- The performance of Configuration-B improves with an increasing Froude number, demonstrating the effectiveness of the modification for the dams with extreme super-critical flow conditions.
- The energy dissipation mechanism of Configuration-B is related to the formation of a complex three-dimensional flow structure, the increase of the turbulent intensity (25-35%), and the optimization of the fluid-structure interaction. This improvement is attributed to the presence of the end sill, which shortens the length of the hydraulic jump by 2.5–4% compared to a free jump, resulting in a stilling basin size reduction [26].
- The pressure distribution on the stilling basin bed for Configuration-B shows a 15–20% reduction, indicating an improved long-term structural durability.

This research significantly contributes to designing a more efficient energy dissipator for dams under extreme flow conditions. It also prepares needed comprehensive empirical data for validating the numerical model and the development of a hydro-dynamics theory about the hydraulic jump on high Froude numbers.

REFERENCES

[1] J. Mulyono, "Konsepsi Keamanan Bendungan Dalam Pembangunan dan Pengelolaan Bendungan," *Jurnal Infrastruktur*, vol. 3, no. 1, pp. 1–62, 2017.

[2] M. Mansyur, Tumpu, F. Rachim, A. Yunianta, and A. Hidayat, "Shape Mode Variation for Structural Health Monitoring: The Case Study of the Bili-Bili Dam in Gowa, South Sulawesi, Indonesia," *Engineering, Technology & Applied Science Research*, vol. 15, no. 3, pp. 23229–23234, June 2025, https://doi.org/10.48084/etasr.10417.

[3] A. Ferrari, R. Vacondio, and P. Mignosa, "High-resolution 2D shallow water modelling of dam failure floods for emergency action plans," *Journal of Hydrology*, vol. 618, Mar. 2023, Art. no. 129192, https://doi.org/10.1016/j.jhydrol.2023.129192.

[4] M. Heidarzadeh and S. Feizi, "A Cascading Risk Model for the Failure of the Concrete Spillway of the Toddbrook Dam, England During the August 2019 Flooding," *International Journal of Disaster Risk Reduction*, vol. 80, Oct. 2022, Art. no. 103214, https://doi.org/10.1016/j.ijdrr.2022.103214.

[5] N. Viti, D. Valero, and C. Gualtieri, "Numerical Simulation of Hydraulic Jumps. Part 2: Recent Results and Future Outlook," *Water*, vol. 11, no. 1, Dec. 2018, Art. no. 28, https://doi.org/10.3390/w11010028.

[6] A. Ghaderi, S. Abbasi, J. Abraham, and H. M. Azamathulla, "Efficiency of Trapezoidal Labyrinth Shaped stepped spillways," *Flow Measurement and Instrumentation*, vol. 72, Apr. 2020, Art. no. 101711, https://doi.org/10.1016/j.flowmeasinst.2020.101711.

[7] E. Afrida, T. Apriyanto, and R. Pujiastuti, "Desain Kolam Peredam Energi Bendung Plaosan Kabupaten Semarang," *Jurnal Teknik Indonesia*, vol. 4, no. 1, May 2023, Art. no. 1, https://doi.org/10.61689/jti.v4i1.414.

[8] A. Habibzadeh, M. R. Loewen, and N. Rajaratnam, "Mean Flow in a Submerged Hydraulic Jump with Baffle Blocks," *Journal of Engineering Mechanics*, vol. 140, no. 5, May 2014, Art. no. 04014020, https://doi.org/10.1061/(ASCE)EM.1943-7889.0000713.

[9] G. M. Abdel Aal, M. Sobeah, E. Helal, and M. El-Fooly, "Improving Energy Dissipation on Stepped Spillways Using Breakers," *Ain Shams Engineering Journal*, vol. 9, no. 4, pp. 1887–1896, Dec. 2018, https://doi.org/10.1016/j.asej.2017.01.008.

[10] A. J. Peterka, *Hydraulic Design of Stilling Basins and Energy Dissipators*. Denver, Colorado, USA: Bureau of Reclamation, 1958.

[11] M. G. Mooselu, M. R. Nikoo, P. H. Bakhtiari, N. B. Rayani, and A. Izady, "Conflict resolution in the multi-stakeholder stepped spillway design under uncertainty by machine learning techniques," *Applied Soft Computing*, vol. 110, Oct. 2021, Art. no. 107721, https://doi.org/10.1016/j.asoc.2021.107721.

[12] W. H. Hager, *Energy Dissipators and Hydraulic Jump*, vol. 8. Dordrecht: Springer Netherlands, 1992.

[13] D. L. Vischer and W. Hager H., *Dam Hydraulic*. Chichester, UK.: John Wiley & Sons, 1998.

[14] H. Chanson, "Introduction: Energy Dissipators in Hydraulic Structures," in *Energy Dissipation in Hydraulic Structures*, H. Chanson, Ed. CRC Press, 2015, pp. 1–9.

[15] S. Damarnegara, W. Wardoyo, R. Perkins, and E. Vincens, "Computational Fluid Dynamics (CFD) Simulation on the Hydraulics of a Spillway," *IOP Conference Series: Earth and Environmental Science*, vol. 437, no. 1, Feb. 2020, Art. no. 012007, https://doi.org/10.1088/1755-1315/437/1/012007.

[16] D. A. W. W. Pratiwi, "Effect of the End Sill to the Stream Pattern in Stilling-Basin," vol. 9, no. 1, pp. 807–819, Jan. 2018.

[17] T. R. Al-Husseini, A.-S. T. Al-Madhhachi, and Z. A. Naser, "Laboratory Experiments and Numerical Model of Local Scour Around Submerged Sharp Crested Weirs," *Journal of King Saud University - Engineering Sciences*, vol. 32, no. 3, pp. 167–176, Mar. 2020, https://doi.org/10.1016/j.jksues.2019.01.001.

[18] S. Dehdar-behbahani and A. Parsaie, "Numerical Modeling of Flow Pattern in Dam Spillway's Guide Wall. Case Study: Balaroud Dam, Iran," *Alexandria Engineering Journal*, vol. 55, no. 1, pp. 467–473, Mar. 2016, https://doi.org/10.1016/j.aej.2016.01.006.

[19] V. Heller, "Scale Effects in Physical Hydraulic Engineering Models," *Journal of Hydraulic Research*, vol. 49, no. 3, pp. 293–306, Jun. 2011, https://doi.org/10.1080/00221686.2011.578914.

[20] F. A. Bombardelli, I. Meireles, and J. Matos, "Laboratory Measurements and Multi-block Numerical Simulations of the Mean Flow and Turbulence in the Non-aerated Skimming Flow Region of Steep Stepped Spillways," *Environmental Fluid Mechanics*, vol. 11, no. 3, pp. 263–288, June 2011, https://doi.org/10.1007/s10652-010-9188-6.

[21] S. Felder and H. Chanson, "Air–Water Flow Patterns of Hydraulic Jumps on Uniform Beds Macroroughness," *Journal of Hydraulic Engineering*, vol. 144, no. 3, Mar. 2018, Art. no. 04017068, https://doi.org/10.1061/(ASCE)HY.1943-7900.0001402.

[22] K. Roushangar, A. Foroudi, and M. Saneie, "Influential Parameters on Submerged Discharge Capacity of Converging Ogee Spillways Based on Experimental Study and Machine Learning-based Modeling," *Journal of Hydroinformatics*, vol. 21, no. 3, pp. 474–492, May 2019, https://doi.org/10.2166/hydro.2019.120.

[23] A. Ghaderi, R. Daneshfaraz, M. Dasineh, and S. Di Francesco, "Energy Dissipation and Hydraulics of Flow over Trapezoidal–Triangular

Labyrinth Weirs," *Water*, vol. 12, no. 7, Jul. 2020, Art. no. 1992, https://doi.org/10.3390/w12071992.

[24] F. D. Sofyan, V. Dermawan, E. Yuliani, " Analisis Komputasi Fluida Dinamis Pada Bangunan Peredam Energi Bendungan Randugunting Kabupaten Blora Provinsi Jawa Tengah," *Jurnal Teknik Pengairan*, vol. 9, no. 2, pp. 82–94, Nov. 2018, https://doi.org/10.21776/ub.pengairan.2018.009.02.2.

[25] W. H. M. Wan Mohtar *et al.*, "Assessment of Dam Appurtenant Structures Under Multiple Flow Discharge Scenarios," *Ain Shams Engineering Journal*, vol. 11, no. 4, pp. 913–922, Dec. 2020, https://doi.org/10.1016/j.asej.2020.03.009.

[26] A. M. Negm, G. M. Aabdel-Aal, A. A. Habib, and Owais, "Effect Of End Sill In Radial Basin On Characteristics Of Free Hydraulic Jumps," in *6th Int. Conf. On Hydro-science and Engineering*, Cairns, Australia, Jun. 2004.